European Journal of Remote Sensing - 2014, 47: 285-305
doi: 10.5721/EuJRS20144718
Received 30/11/2013, accepted 24/03/2014

European Journal of Remote Sensing
An official journal of the Italian Society of Remote Sensing
www.aitjournal.com

Correcting MODIS 16-day composite NDVI time-series with actual acquisition dates

Stefano Testa[1]*, Enrico C. Borgogno Mondino[1] and Chiara Pedroli[2]

[1]Department of Agricultural, Forest and Food Sciences
Via L. da Vinci 44, Grugliasco (TO) - Italy
[2]Montagnard s.r.l. Via Circonvallazione 119/A, Verrès (AO) - Italy
*Corresponding author, email address: stefano.testa@unito.it

Abstract
Remote sensing phenological works often use vegetation index (VI) time-series (TS). Since ground-observed phenological metrics occurrences vary by a few days from year to year, TS temporal accuracy became mandatory, but it is less strict in composite data. A technique to recover the temporal accuracy of 250 m 16-day composite VI from the MODIS MOD13Q1 product is proposed, relying on acquisition dates contained in the Composite day of the year layer. We demonstrated that the correction process significantly affected the VI TS during most of the year, especially in spring and autumn when the starting of season (SOS) and the end of the season (EOS) are expected. As a consequence of the TS correction process, SOS estimation showed to be affected too.
Keywords: Composite day of the year, MOD13, phenology, climate change, TIMESAT.

Introduction
The United States International Biological Program (US/IBP) committee defined phenology as the study of the timing of recurring biological events, the causes of their timing with regard to biotic and abiotic forces, and the interrelation among phases of the same or different species [Lieth, 1974]. Phenology is considered a good indicator of environmental variations induced by climate change, as found in earlier studies [Fabian and Menzel, 1998; Schwartz, 1998; Bradley et al., 1999]. It was found to be driven by climate behavior [Peñuelas and Filella, 2001; Crucifix et al., 2005; Schucknecht et al., 2013] and to concurrently affect the climate system [Peñuelas et al., 2009; Richardson et al., 2013; Stroppiana et al., 2014]. Several works showed the biogeochemical cycles to be affected by phenology [Gu et al., 2003; Cowie, 2007; Noormets, 2009] and, because of this, accurate estimation of phenological season become important when dealing with their temporal features. Because remote sensing plays an important role in understanding large area seasonal events [Reed et al., 2003], it is important to have good data on which to base analysis.
Vegetation indices (VIs) are the most appreciated solution in remote sensing of vegetation since they are more stable and meaningful than single bands [Soudani et al., 2008]. In

order to make satellite-derived phenological metrics reliable and qualitatively comparable with the ones observed in field measurements, VIs values are required to have good temporal resolution [Soudani et al., 2008] and alignment. In fact, field surveys showed little inter-annual variability in field-measured phenological metrics. Brügger et al. [2003], studying Fagus sylvatica phenophases between 1991-1999 in four Swiss test sites, found differences in leaf unfolding dates between the first and the last tree of each sample plot ranging between 7.1 and 14.3 days, depending on the test site (5 to 11 trees were sampled per test site). Nordli et al. [2008], evaluating the bud burst date of different species over four sites in Norway on multi-decadal time-series (TS), found bud burst anticipation trends ranging from -0.2 to -5.1 days per decade, corresponding to -0.7 to -17.8 days as absolute difference from the average bud burst day over 35 years. Magnitude and trends of vegetation phenology variations are reported in Richardson et al. [2013].

The 16-day composite MODIS VIs product (MOD13Q1) at 250 m are widely used in phenological and vegetation dynamics surveying works, e.g. Ahl et al. [2006], Karlsen et al. [2008], Boschetti et al. [2009], Colombo et al. [2009], Karlsen et al. [2009], Busetto et al. [2010], Colombo et al. [2011], Xu et al. [2011], Song et al. [2013]. MOD13Q1 provides one image every 16 days (23 images per year), usually without missing data (see MOD13Q1 dataset paragraph for details). VI TS generated from this product are less noisy than daily data and allow easier processing [Hmimina et al., 2013]. A known problem is related to the discontinuities generated by the compositing process [Solano et al., 2010]. In fact, despite composite images being nominally equidistant in time (one image every 16 days), VI values can be acquired in each day of the 16-day compositing period to which they refer, and the actual temporal distance between adjacent VI values can vary from 1 to 32 days, depending on the dates of acquisition of the reflectances used to compute the VI. Such an uncertainty in the temporal location of the VI values is much greater than the variations of phenological metrics measured in the field and reported in the above cited works. In addition, wrong VI value positions affect the shape of the fitting function used to estimate the phenological metrics of interest and this can make remote sensing results not precisely comparable with ground data due to loss of precision. Obviously, works based on daily data are not affected by this trouble [Soudani et al., 2008; Hmimina et al., 2013]. Starting from Collection 5 of the MOD13Q1 product, a new layer, named Composite day of the year (CDOY), was released. It contains, per pixel, the date of acquisition of the reflectances used in VIs computation, allowing for TS calibration [Solano et al., 2010].

The first objective of this work was to approach the problem of VIs TS temporal features and to propose a technique to generate uniform, temporally-corrected TS of MOD13Q1 VIs well-suited for phenological studies. The first problem to solve in this procedure, the lack of a reference date for NDVI values, was overcome by studying the temporal pattern of acquisition dates from the CDOY layer. Knowing the nominal date VI values were referable to, it was possible to carry out the TS correction process by: a) interpolating the VI values previously moved to their actual acquisition date and b) resampling the interpolating function to the nominal reference date. The second objective of this work was the numerical comparison of the corrected TS with the original one (both after being fitted with the TIMESAT double-logistic function) in order to evaluate if the correction process significantly affected the TS or not. Third, in order to evaluate if and how the TS correction process affected the estimation of phenological metrics (e.g. SOS), SOS estimations operated with both the corrected and the not-corrected TS were compared.

Study area

The study area is ascribable to the Piemonte region (Fig. 1). The region extends over 25,402 km^2 in NW Italy. Its morphology is very diverse with mountains, hills and flat areas; these geographic features represent respectively 43.3%, 30.3% and 26.4% of the region's area. On the west and north sides, the Piemonte region is surrounded by the Alps; on the south side the Apennines separate the region from the Mediterranean (Ligurian) sea. Eastward it opens onto the Padana flat. In the middle of the region, a group of hills is present.

Test area

Tests were focused on the *Castanea sativa* (chestnut) pure stands within the Piemonte region. Chestnut stands were identified using the Piemonte region Forest Map (Fig. 1), derived from the Piemonte region *Forest Management Plans*. Further details about the forest map are given in section 3. Available DataLand cover dataset.

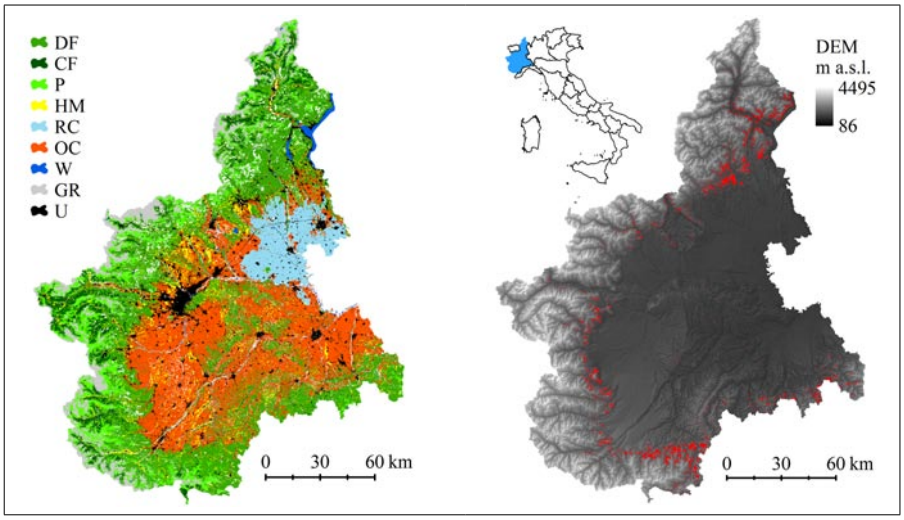

Figure 1 - Left: a simplified version of the LCM: the original 51 classes were aggregated into 9 more generic ones. DF: deciduous forests, CF: coniferous forests, P: pastures, HM: hay meadows, RC: rice crops, OC: other crops, W: water bodies (rivers, lakes), GR: glaciers and rocky lands, U: urban areas. Right: test area. In red color are the pure 7,969 pixels selected as test area for this study. Background: SRTM 90 m DEM. In the small frame: Italy (scale: 1:40,000,000) and, in light blue, the Piemonte region. Both images of the Piemonte Region have been generated to 1:3,000,000 scale.

Chestnut stands extend over 204,364 ha in the Piemonte region; they represent 23% of the regional forest surface and are the most extensive stands. Piemonte region's chestnut stands are little invaded by other tree species because of their active management that controls the natural chestnut trend to mix with other species [Gottero et al., 2007]. In fact, 89% of chestnut stands are actively managed and 5% are reserved for fruit production [Gottero et al., 2007]. As a consequence, their composition is rather pure, 80% on average (4 trees out of 5 are chestnut). This situation, mainly related to stands' active management, is favorable for remote sensing phenological studies. Moreover, chestnut stands' hosting ground is

commonly covered by a thick layer of leaves which mostly prevents grass growth: this is expected to improve spring signal purity.
80% of the pixels covering the whole Piemonte Region and 76% of the ones corresponding to chestnut stands are mixed because of the moderate spatial resolution of the MOD13Q1 data (250 m). Since mixed pixels' signal is not pure and the accuracy of land-cover monitoring is reduced [Pena-Barragan et al., 2011; Wang et al., 2012], mixed pixels were not considered for this study. Finally, 7,969 pure pixels (49,806 ha, 24% of the original extent) were selected. To validate purity conditions of the selected pixels, a visual inspection of some areas was performed using Google Earth [Soudani et al., 2008], and a good match was found between the selection and the ground vegetation.

Available Data

MOD13Q1 dataset

Time-series of the MODIS MOD13Q1 product (Vegetation Indices 16-Day L3 Global 250 m) over the period from January 2001 to December 2011 (11 years, 253 images) have been used in this work. The dataset provides two VIs layers: Normalized Difference Vegetation Index (NDVI) and Enhanced Vegetation Index (EVI). The first one represents the continuity with the Advanced Very High Resolution Radiometer (AVHRR) mission; the second one is a newer VI, which is known to be able to account for both background and aerosol effects [Huete et al., 2002; Soudani et al., 2008]. This study was focused on NDVI because it is widely used in phenological works, e.g. Boschetti et al. [2009], Colombo et al. [2011], Soudani et al. [2008], Hmimina et al. [2013], and because it is known to be more sensitive to small increases in the amount of photosynthetic vegetation [Soudani et al., 2006; Soudani et al., 2008; Sesnie et al., 2012]. Moreover, the authors themselves in previous unpublished tests found that NDVI performed better when classifying low-vegetated sample areas. Nevertheless, it suffers from problems related to background and path radiance effects and saturation especially over dense canopies [Jackson and Huete, 1991; Huete et al., 2002]. *Pixel reliability* (PR) and CDOY layers, supplied with the MOD13Q1 collection 5, were considered for NDVI TS calibration. The PR layer defines the overall quality of the NDVI value of each pixel, giving information about its status, as explained in Table 1. This information was used in TIMESAT [Jönsson and Eklundh, 2002, 2003, 2004] to weigh NDVI values according to their quality: the lower the weight, the less the NDVI value affects the estimation of the function fitting parameters since a greater uncertainty is assigned to it [Jönsson and Eklundh, 2004]. The weights were assigned arbitrarily [Jönsson and Eklundh, 2004], since no indication was available from the scientific bibliography. Table 1 is taken from Solano et al. [2010] except column (4).

Table 1 - MOD13 Pixel Reliability flags and corresponding quality.

Rank Key	Summary QA	Description	Weight assigned in TIMESAT
-1	Fill/No Data	Not Processed	n.a.
0	Good Data	Use with confidence	1.00
1	Marginal data	Useful, but look at other QA information	0.90
2	Snow/Ice	Target covered with snow/ice	0.90
3	Cloudy	Target not visible, covered with cloud	0.15

The CDOY layer was crucial for this work. It contains, for each pixel of the image, the day of the year in which reflectances used in the VIs computation were acquired; this information permitted us to calibrate NDVI TS in time, i.e., to place NDVI values in their exact position along the TS.

MOD13Q1 dataset compositing algorithm

A basic requirement for robust phenological works is the possibility of processing internally coherent images (coeval, meaning that all values refers to the same date) regularly distributed along dense TS. When working with composite data, this condition is missing. In fact, any compositing process involves temporal and spatial "discontinuities, which are inevitable and result from the fact that disparate days can always be chosen for adjacent pixels over the 16-days period. Thus, adjacent selected pixels may originate from different days, with different sun-pixel-sensor viewing geometries and different atmospheric and residual cloud/smoke contamination" [Solano et al., 2010]. Figure 2, generated with a sample from the study dataset, shows the effect of the compositing process. Observations refer to the compositing period (image) #16 of 23 of the year 2004. The compositing period #16 theoretically embraces dates from the 28th of August (day of year (DOY) 241) to the 12th of September (DOY 256); as shown, acquisition dates actually range from DOY 241 to 252. This condition determines the necessity of a calibration process aimed at transforming raw data TS into new more suitable TS.

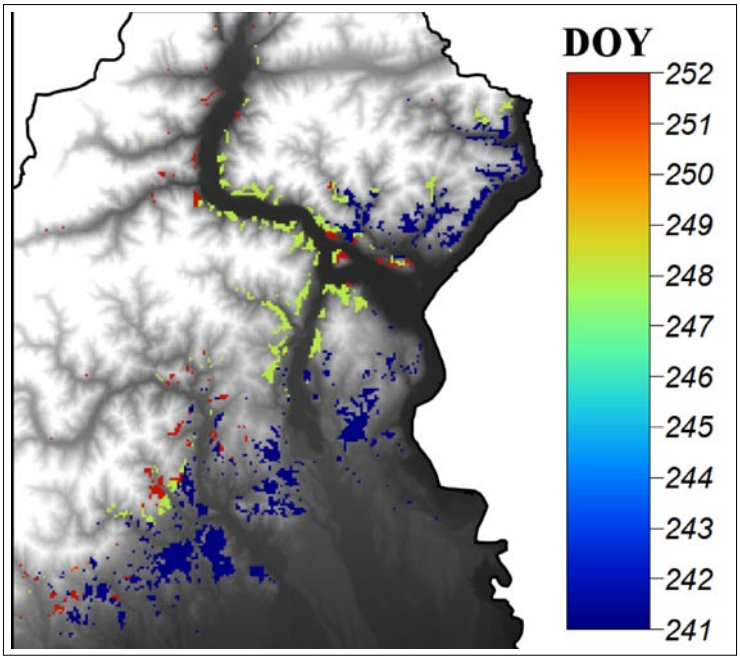

Figure 2 - Effect of the compositing process in the northern part of the test area (about 40 x 40 km). Background: SRTM DEM [Jarvis et al., 2008].

The MOD13Q1 16-days composite product is obtained by selecting for each pixel the best observation that occurred in the 16-day reference period. All the available images are compared according to a Quality Assurance (QA) filtering criterion that takes care of signal quality, cloud contamination and viewing geometry. Nadir and cloud-free pixels have the best QA rank. The number of images falling in the 16-day reference period ranges between 0 and 64 (1 to 4 acquisitions a day are possible; persistent cloudiness causes poor observation quality). Usually, the number of good quality images varies between 1 and 5 per period and in general decreases from the poles toward the equator. When the best images have been selected, two compositing strategies can be applied. If the number of well-ranked images is two or more, the compositing strategy is the *Constraint View angle – Maximum Value Composite* (CV-MVC), which selects the closest-to-nadir acquisition. Otherwise, the number of available acquisitions (without considering their QA rank) is evaluated; if it is more than one, the classic *Maximum Value Composite* (MVC) technique is applied selecting the image in which the highest NDVI value occurred. If a certain position has no good acquisition available, the correspondent pixel is filled with the historic average value: this is the reason why no missing data can be found in any TS image.

Land cover dataset

The forest map of the Piemonte region was used to identify MOD13Q1 pixels corresponding to the desired forest class. It was produced, mainly from field surveys, in order to support the management politics of the region's agricultural, forest, and pasture areas between 1999 and 2004 and has been partially updated in 2012. This data was produced at a nominal scale of 1:25,000 and is freely available for users in vector format on the cartographic portal of the Piemonte region (http://www.sistemapiemonte.it/montagna/sifor/). The original vector file was gridded according to the MOD13Q1 images generating a raster land cover map (LCM) with 250m geometric resolution (comparable with a 1:1,250,000 scale map).

Methods

Determination of nominal acquisition dates

The first objective of this work was the identification of one reference (or nominal) acquisition date (NAD) to use during the following TS processing. In fact, each NDVI value from MOD13Q1 product refers to a compositing period, not to a specific date. First, original NDVI layers were stacked in a 253 image-long TS (23 images/year x 11 years). NAD represents the date, inside each 16-day compositing period, assigned to the NDVI value representing the whole period itself. Actual acquisition dates of raw NDVI values are stored in the CDOY layer. Jointly considering all the pixels from the test area of each CDOY layer belonging to the TS, 253 median values of the acquisition dates (MEADs) and the correspondent interquartile ranges (IQR) were calculated. Median was used in place of mean value because the population of the acquisition dates was not expected to be normally distributed. IQR was elected to represent the dispersion of MEADs since the distribution was not symmetric [Rousseeuw and Croux, 1993]. To describe the MEADs temporal pattern, observations were aggregated by: a) 16-days compositing period; b) month; c) season; and, d) year. Each aggregation occurs over a different number of units: 23 for a); 12 for b); 4 for c); and, 11 for d). To synthesize information, the median of all MEADs was calculated. The details of aggregation are available in Table 2.

Table 2 - 1: Composite periods of the MOD13 year; 2: first day of each compositing period; 3,4: Julian day to Gregorian dates, 5: corresponding season. Underlined: compositing periods involved in the composition of the October and November months and differences between leap and non-leap years.

(1) Composite #	(2) CDOY	(3) Non-leap years	(4) Leap years	(5) Season
1	1	01-Jan	01-Jan	Winter
2	17	17-Jan	17-Jan	
3	33	02-Feb	02-Feb	
4	49	18-Feb	18-Feb	
5	65	06-Mar	05-Mar	
6	81	22-Mar	21-Mar	Spring
7	97	07-Apr	06-Apr	
8	113	23-Apr	22-Apr	
9	129	09-May	08-May	
10	145	25-May	24-May	
11	161	10-Jun	09-Jun	
12	177	26-Jun	25-Jun	Summer
13	193	12-Jul	11-Jul	
14	209	28-Jul	27-Jul	
15	225	13-Aug	12-Aug	
16	241	29-Aug	28-Aug	
17	257	14-Sep	13-Sep	
18	273	30-Sep	29-Sep	Autumn
19	289	16-Oct	**15-Oct**	
20	305	**01-Nov**	**31-Oct**	
21	321	**17-Nov**	16-Nov	
22	337	03-Dec	02-Dec	
23	353	19-Dec	18-Dec	

Some considerations can be made at this point. A) In leap years, CDOY refers to different dates after Julian day 60 (29th of February, image 4 of 23, Table 2). In order to compare leap and non-leap years accurately, CDOY from leap years greater than or equal to 60 was corrected by subtracting 1. Considering both 2004 and 2008 together (the only leap years in the 2001 – 2011 TS), 110 values were moved from the 29th of February to the 28th of February (0.005% of the total number of values), which can be considered a negligible amount, as well as the 168 values that had been actually acquired on the 28th of February. B) MOD13 years are longer than 365 or 366 days; in fact, 23 compositing periods/year x 16 days/compositing period = 368 days/year. Because of this, acquisition dates in the last image of each year (the 23rd) may be greater than 365 (366 in leap years). Those values stepping over this threshold falls in the first days of the following year: for this, their actual value may range between 1 and 3 (2 in leap years) instead of between 366 (367 in leap years) and 368. This fact results in CDOY values that must be corrected in order to avoid incorrect MEADs calculation. We accounted for this problem by adding 365 (or 366) to CDOY values

belonging to the last image of each year if their value was less than 353, the minimum value possible. C) As shown in Table 2, in non-leap years, October is represented by only one image (not two as it would normally be), while in leap years this situation happens in November; this was considered when calculating monthly MEADs. D) In order to make Julian dates comparable throughout the year, CDOY values were rescaled as follows:

$$CDOY_{i,j,t\,CP} = CDOY_{i,j,t} - 16 \cdot (CP - 1) \quad [1]$$

where CP is the CP^{th} compositing period of the year and $CDOY_{i,j,t}$ is the value of the CDOY stack at the position i,j,t. As fully explained in the *Results* section, the nominal MEAD was set to 9.

Generation of the date-corrected TS

Each value read from the $NDVI_{ORIGINAL}$ TS was moved to its proper acquisition date (read from the CDOY TS) obtaining a new TS, $NDVI_{REAL}$, in which values were not equidistant. This is evidenced by the green dots in Figure 3 that are shifted horizontally, backward or forward, respective to the nominal position they refer to (the closest red dot) that are instead equidistant to each other. The $NDVI_{REAL}$ TS was then interpolated using a cubic spline interpolation [Hmimina et al., 2013] and, finally, re-sampled to each 9th day. This process generated a new, coherent and temporally equidistant TS, NDVI-9_{RAW}, where the "horizontal shift" (temporal shift) of $NDVI_{REAL}$ values was converted into "vertical shift" (NDVI shift). As shown in Figure 4, NDVI-9_{RAW} blue dots are equidistant, as well as the $NDVI_{ORIGINAL}$ red dots, but NDVI values are different. In Figure 5 $NDVI_{REAL}$ and NDVI-9_{RAW} are compared: the plot makes clear the sampling of the cubic spline function done to 9th days. It is evidenced by the blue dots that are in correspondence of the vertical gridline, which depicts the 9th days of each compositing period.

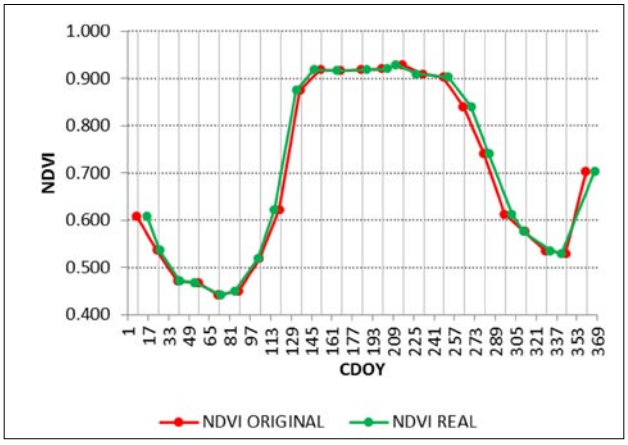

Figure 3 - Comparison between $NDVI_{ORIGINAL}$ (nominally equidistant NDVI values) and $NDVI_{REAL}$ TS (irregularly distanced NDVI values). Plotted data are from the pixel centered over 4,911,250 N 426,250 E UTM WGS84 32N and belongs to the year 2004; Figure 4. Figure 4 and Figure 5 plots refer to this same pixel/year.

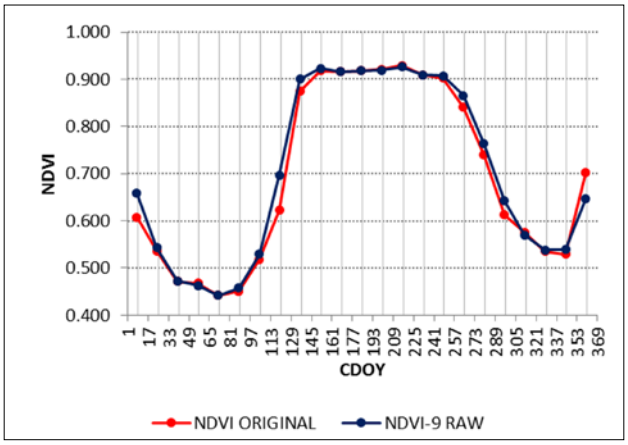

Figure 4 - Comparison between $NDVI_{ORIGINAL}$ and $NDVI\text{-}9_{RAW}$.

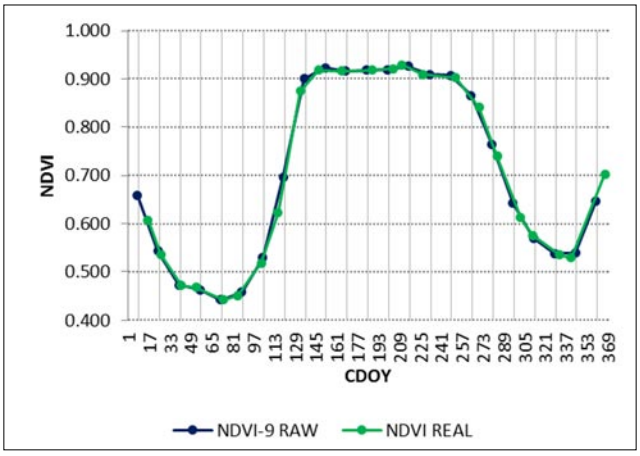

Figure 5 - Comparison between $NDVI\text{-}9_{RAW}$ and $NDVI_{REAL}$.

TS smoothing

$NDVI_{ORIGINAL}$ and $NDVI\text{-}9_{RAW}$ TS were smoothed using the procedure available in TIMESAT 3.1.1. This operation, retained to improve data quality by reducing signal noise along TS [Gutman et al., 1995], generated two new TS, respectively called $NDVI_{SMOOTH}$ and $NDVI\text{-}9_{SMOOTH}$. The selected smoothing function was the logistic one, well described in Jönsson and Eklundh [2004] because of its good performances in terms of noise reduction [Hird and McDermid, 2009] and seasonality detection [Soudani et al., 2008; Hmimina et al., 2013]. It is well suited to describe the deciduous-tree growth cycle that is driven by the cumulative temperature, which can be represented as a logistic function of time [Zhang et al., 2003]. The algorithm was set to run 2 envelope iterations with low adaption strength to high values (2 of 10) in order to avoid over-estimation of highest values. In fact, MODIS NDVI saturation is a known problem related to the reduced width of the red band (620-670 nm, 50 nm) if compared with the previous AVHRR

(580-680 nm, 100 nm) and TM/ETM+ (630-690 nm, 60 nm) ones. This fact makes MODIS NDVI too sensitive to chlorophyll content and easier to saturate [Elvidge and Chen, 1995; Huete et al., 1999]. Smoothing was run weighing NDVI values according to the correspondent PR ranking (Table 1). Successively, TIMESAT itself was used to calculate the per-pixel starting of season (SOS) for each of the eleven years of both $NDVI_{SMOOTH}$ and $NDVI\text{-}9_{SMOOTH}$ TS, obtaining two 11-images-long SOS TS of the test area. These TS were then compared in order to evaluate how the date-correction procedure affected the SOS estimation.

NDVI TS comparison

Comparison of the $NDVI_{SMOOTH}$ and $NDVI\text{-}9_{SMOOTH}$ TS was done for each unit belonging to the four above mentioned temporal bases (23 compositing periods, 12 months, 4 seasons, 11 years). The [$NDVI_{SMOOTH}$ - $NDVI\text{-}9_{SMOOTH}$] array of NDVI differences (hereafter called DA) was generated for each unit. NDVI median difference (MD), median absolute deviation of differences (DMAD), IQR and Root Mean Square Error (RMSE) were computed. MD is the median of the DA, DMAD is its median absolute deviation (MAD), and RMSE is calculated as:

$$RMSE = \sqrt{\frac{\sum_1^n (DA)^2}{n-1}} \quad [2]$$

where n is the number of elements composing the DA difference array.

MD represents the bias induced in the TS by the correction process for the considered temporal unit. DMAD represents the dispersion of NDVI values around their MD. RMSE represents the overall difference between the examined TS. For each temporal basis, an image stack was generated (the number of bands corresponds to the number of units). In order to synthesize results concerning the entire forest class, median values of the previously generated metrics were computed for each temporal unit.

Estimation of Starting of Season

SOS was estimated in TIMESAT for all of the 11 years (2001-2011) at each pixel of the test area. The threshold-based approach was used and we set a threshold value of 0.25; it means that the SOS date is the one where the fitting function value has increased by 25% respective to the closest leftward minimum. The temporal window where the SOS date should be searched was 28 images-wide (23 images of the considered year plus the last 5 images from the previous year), according to the TIMESAT user manual suggestion. The impact of using date-corrected TS on SOS estimation was evaluated comparing results obtained by processing separately the $NDVI_{SMOOTH}$ and $NDVI\text{-}9_{SMOOTH}$ TS. A SOS difference image (ΔSOS) was generated for every year. The resulting relative and cumulated frequency histograms were then assessed and compared. SOS could not be calculated for every pixel/year in case the fitted function had not increased enough to pass the input threshold. This occurred over a variable amount of pixels, despite the 5-image buffer (~2.5 months) before each considered year. Thus, just those pixels where SOS of the y^{th} year were available for both TS were taken into consideration. The number of available pixels (AP) for statistics computation ranged between 65% and 98% of the 7,969 ones, depending on the considered year. In order to determine significant ΔSOSs, two theoretical precision levels were set, respectively ±7 days and ±2 days. The first level corresponds to

the theoretical time lag between successive field observations of the RENECOFOR (*REseau National de suivi à long terme des ECOsystèmes FORestiers*) phenological network [Soudani et al., 2008]; the second is the field observation frequency reported in Liang et al. [2011]. ΔSOS lower than or greater than the theoretical precisions were considered significant.

Results

MEAD analysis

In this work, one nominal date to refer to the NDVI values was needed in order to carry out the correction process of the $NDVI_{RAW}$ TS. Figure 6 shows that MEAD values were close to the center of each 16-day period during most of year. The only MEADs more distant than ± 3 days from the nominal MEAD were registered on compositing periods #19 and #21. The bar plot in Figure 7 is the frequency histogram of the MEAD series in the plot *Compositing period #* in Figure 6. Figure 7 shows that acquisition dates mostly occur at every 9th day of the 253 analyzed compositing periods; for this reason the nominal (or reference) MEAD was set to 9.

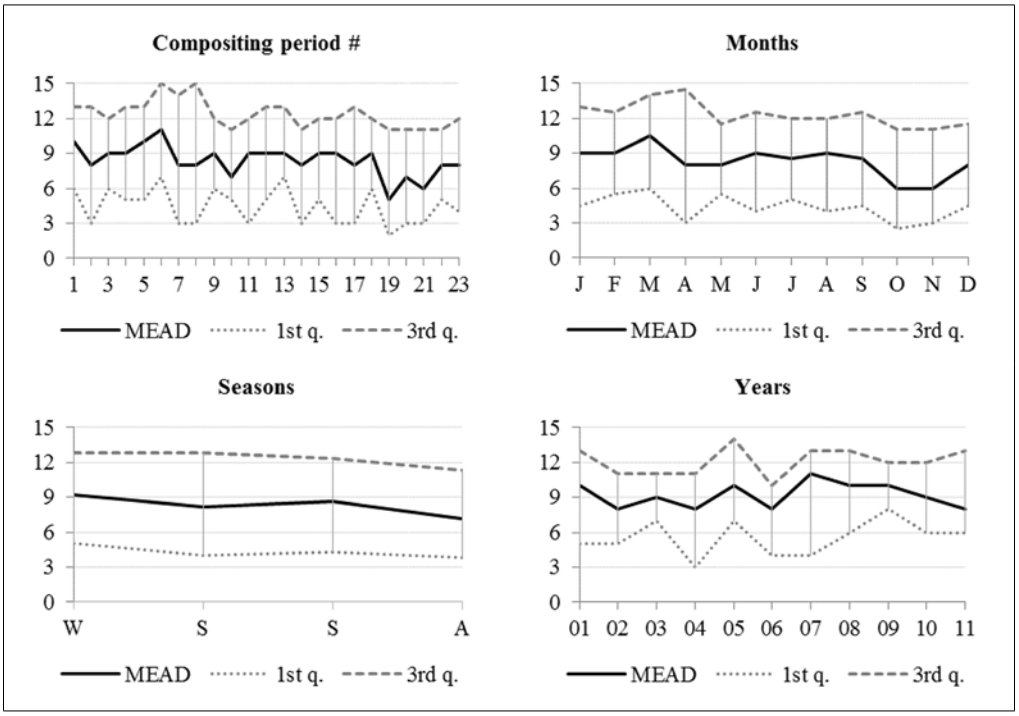

Figure 6 - MEADs averaged over the four temporal bases. Unit of measurement of vertical axis is days in all plots.

This result was confirmed by the modal value calculated using all the test area pixels belonging to the 253 CDOY layers. Seasonal variability was very reduced, with an expected negative peak in autumn, while the inter-annual variability was quite irregular. MEAD distribution was asymmetric as the IQR boundaries state. This confirmed that the adoption of IQR instead of ±MAD was a correct choice.

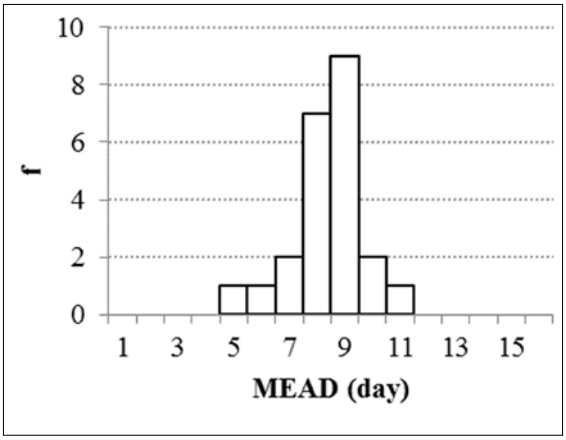

Figure 7 - Frequency histogram of the *MEAD* series of Figure 6 - *Compositing period* #. The modal value occurred on the 9th day.

NDVI TS comparison

$NDVI_{SMOOTH}$ and $NDVI\text{-}9_{SMOOTH}$ TS were compared in order to evaluate how the correction process affects the TS itself. MD and RMSE were both calculated: while MD represents median positive or negative TS differences, RMSE stands for the overall magnitude of errors. Figure 8 shows that MDs were close to zero most of the year; the largest anomalies were found in the compositing periods #19 and #20, where the maximum difference between actual and nominal MEAD was previously observed. NDVI difference values were less than ±0.025, the MOD13 NDVI declared accuracy [MODIS Land Team, 2011]. Such accuracy is defined as the capability of the composite NDVI to retrieve a top of canopy and nadir VI value using high quality results (clear, low aerosol, sensor view angle less than 30°) [MODIS Land Team, 2011]. No MD value was higher than this accuracy threshold along any temporal aggregation. DMAD peaks in compositing periods #8 and #20 are the consequence of an amount of pixels highly affected by the TS correction procedure that is greater in those temporal units (i.e. compositing periods) than in others. Simultaneously, at those units, MDs assumed extreme values in more pixels than in other temporal units. From this point of view, mid-May to mid-September NDVI values were negligibly affected by the correction process, since both MD and DMAD were very low and below the NDVI sensibility threshold. Moreover, as shown by the MD autumnal peak, $NDVI\text{-}9_{SMOOTH}$ values tended to be lower than $NDVI_{SMOOTH}$ ones in the period from mid-October to mid-November. Both MD and DMAD were almost constant along the considered eleven years.

Figure 9 is concerned with the RMSE temporal behavior. It shows that the compositing periods from #10 to #17 (end-May to mid-September) were the only ones characterized by: a) RMSE values less than the MODIS NDVI sensitivity threshold; and, b) very low dispersion (as shown by the IQR range boundary lines). Out of this temporal interval, the RMSE and IQR behaviour is opposite. This is very evident in the season-based plot. The periods #7 and #8, representing the 32 days from April 7th to May 8th had the highest RMSE peak. The inter-annual variability was very low but always greater than the sensibility threshold.

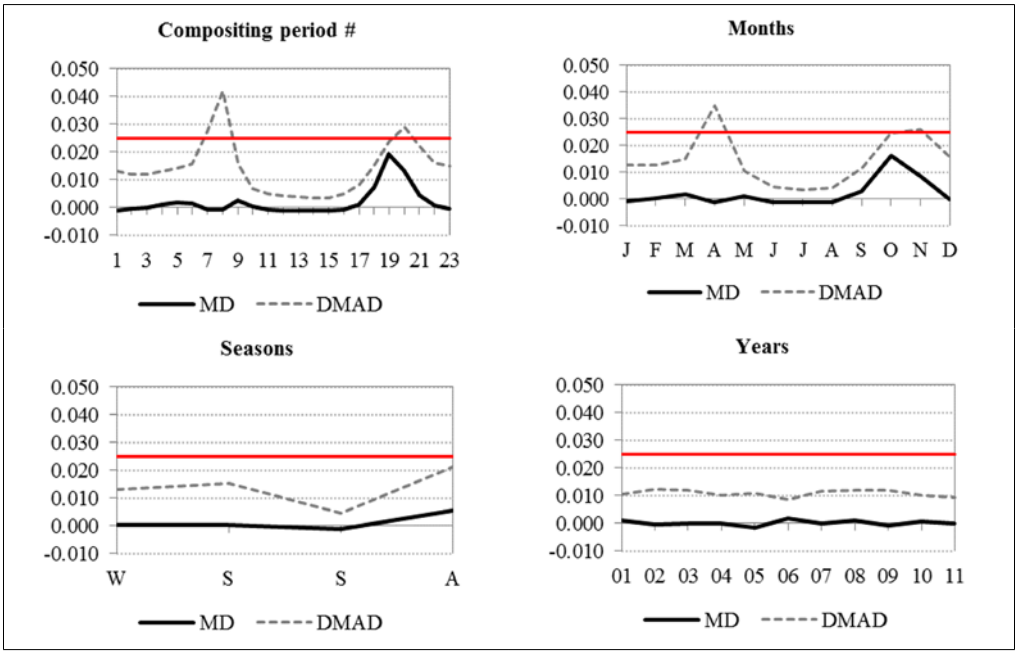

Figure 8 - NDVI median values of MD [$NDVI_{SMOOTH}$ - $NDVI\text{-}9_{SMOOTH}$] and correspondent DMADs plotted over the four reference time bases. Unit of measurement of vertical axis is *NDVI* in all plots. The red line represents the MOD13Q1 NDVI sensibility threshold (NDVI = 0.025).

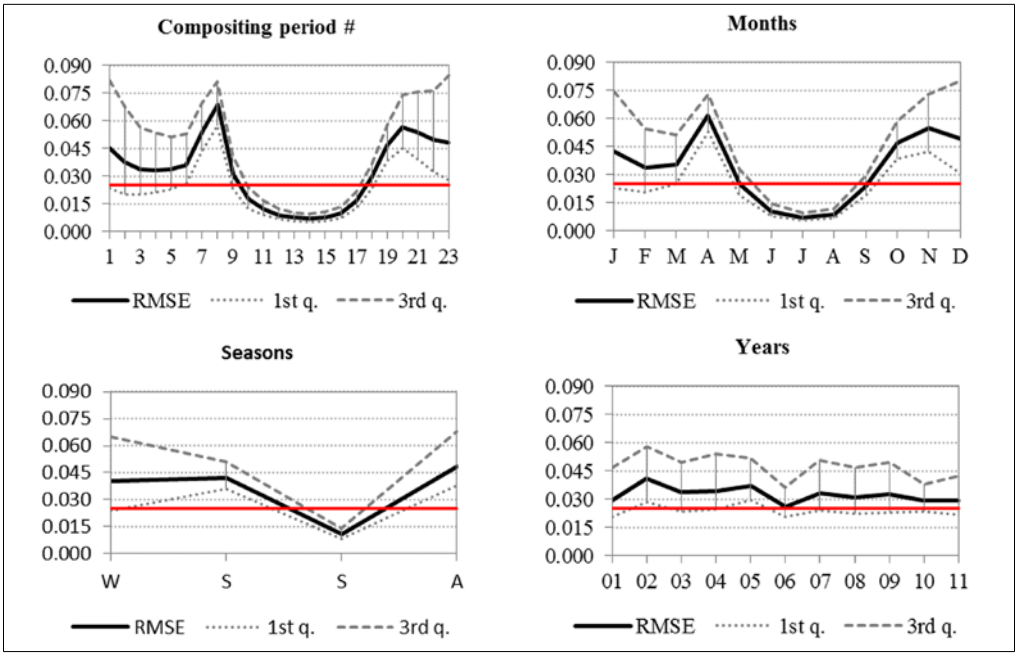

Figure 9 - RMSE medians plotted over different time bases. Unit of measurement of vertical axis is *NDVI* in all plots. The red line represents the MOD13Q1 NDVI sensibility threshold (NDVI = 0.025).

Starting of season dates

Figure 10 reports frequency histograms of the eleven ΔSOS images [SOS NDVI-9$_{SMOOTH}$ – SOS NDVI$_{SMOOTH}$]. Both relative and cumulated frequencies are reported. Red solid lines do not reach 100% since the only differences between -30 and +30 days were considered.

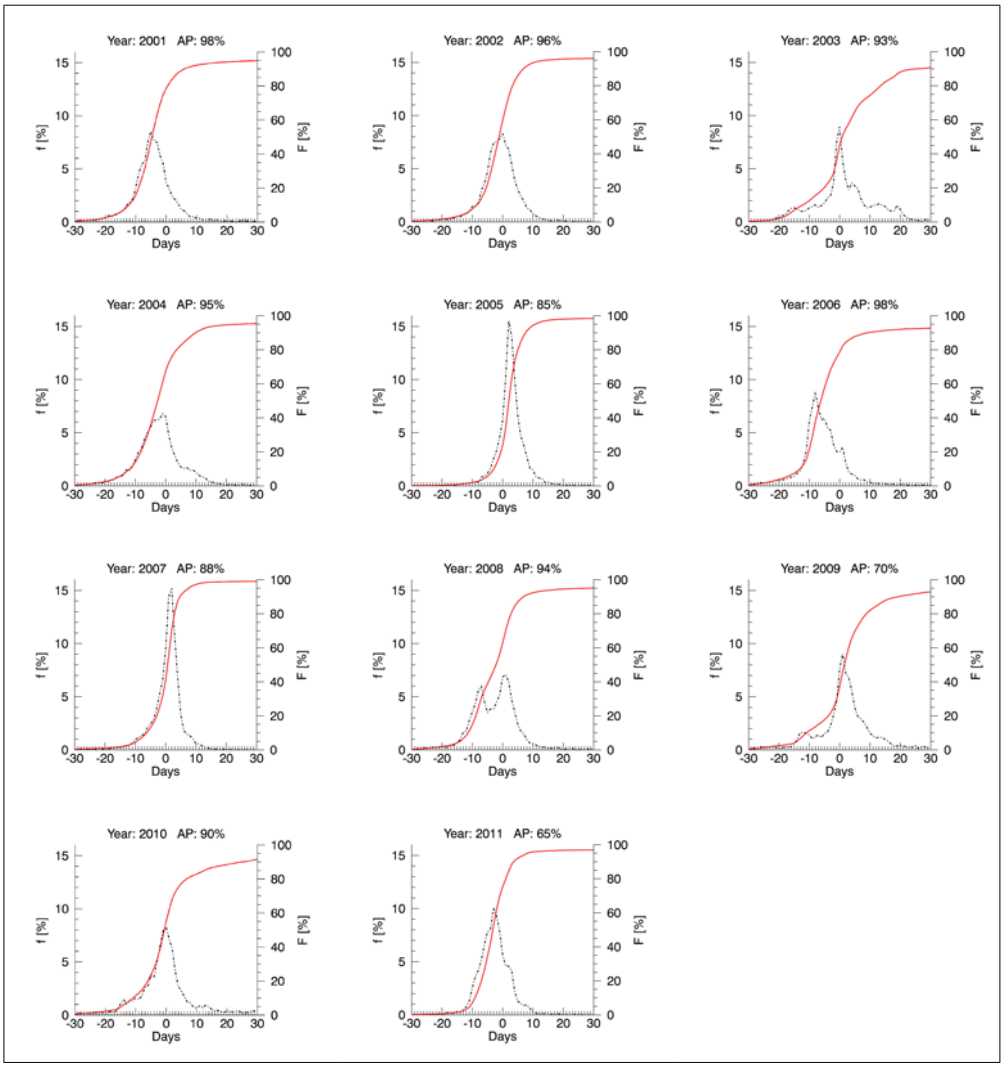

Figure 10 - Relative frequency histograms of [SOS NDVI-9$_{SMOOTH}$ – SOS NDVI$_{SMOOTH}$] ΔSOS images for the eleven considered years. Dash-dot black lines: relative frequencies (left axis); red solid lines: cumulative relative frequencies histograms (right axis). Solid lines do not reach 100% since only differences between -30 and +30 days where considered. In chart titles: AP: available pixels (pixels where SOS was found in both NDVI-9$_{SMOOTH}$ and NDVI$_{SMOOTH}$ images).

The amount of available pixels (pixels where SOS was found in both NDVI-9$_{SMOOTH}$ and NDVI$_{SMOOTH}$ images) was reported (AP label) in each plot. Annual histograms appeared

to be different in terms of symmetry and position. In order to synthesize the histograms' content, an extract is reported in Figure 11: the amounts of pixels where ΔSOS was greater than the ±7 days and the ±2 days precision levels are reported for every year. As shown in Figure 11, the amount of significant ΔSOS varies greatly from year to year and depending on the precision level, ranging from 2% to 31% if the accepted error is ±7 days and between 48% and 84% if referring to the ±2 days precision level.

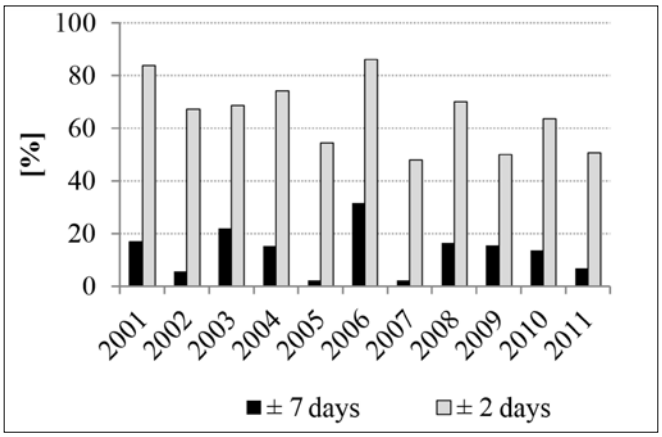

Figure 11 - Significant ΔSOS. ±7 and ±2 days are the precision levels. Values are referred as percentage of the test area.

The time embraced by the compositing periods #7 and #8, when the RMSE peak fell, is the time of the year when the impact of the correction process is greater. Because of this, SOS occurring during these compositing periods were expected to show greater ΔSOS values as a consequence of the greater diversity between $NDVI_{SMOOTH}$ and $NDVI\text{-}9_{SMOOTH}$ TS (i.e. greater RMSE). To evaluate ΔSOS values, histograms of SOS referring to the corrected TS ($NDVI\text{-}9_{SMOOTH}$) were generated (Fig. 12). The plot in Figure 13 shows an extract representing the frequencies 7 and 8 (i.e. compositing periods #7 and #8), which are the ones falling within the April RMSE peak: 0% to 20% of the estimated SOS fell within such peak, depending on the year.

Discussion

The rationale of this work is that erroneous temporal positions of NDVI values along TS can affect pixel phenology interpretation. In fact, raw composite products, such as the MOD13Q1 one, generate a deformed time sequence of NDVI observations. This fact, especially when trying to accurately estimate phenological parameters, can lead to erroneous results. In this paper, the authors proposed a technique for temporal correction of MOD13Q1 VI TS using the CDOY layer information and described the effects of such a process in terms of TS absolute (MD) and global (RMSE) differences. As a side topic, effects of TS correction in SOS estimation were assessed, comparing results obtained from corrected and uncorrected TS. The reference MEAD of the test dataset, computed from the CDOY images, was 9. This

value was close to the centre of the 16-day compositing periods and was used to recalculate NDVI values according to interpolation given by the spline fitting function. Results showed that, considering the entirety of the test area, no significant bias was introduced by the correction process. Nevertheless, the spring and autumnal peaks in DMAD values is much higher than the 0.025 NDVI sensitivity threshold: this leads us to consider that a large amount of pixels may be affected by significant bias in these time periods.

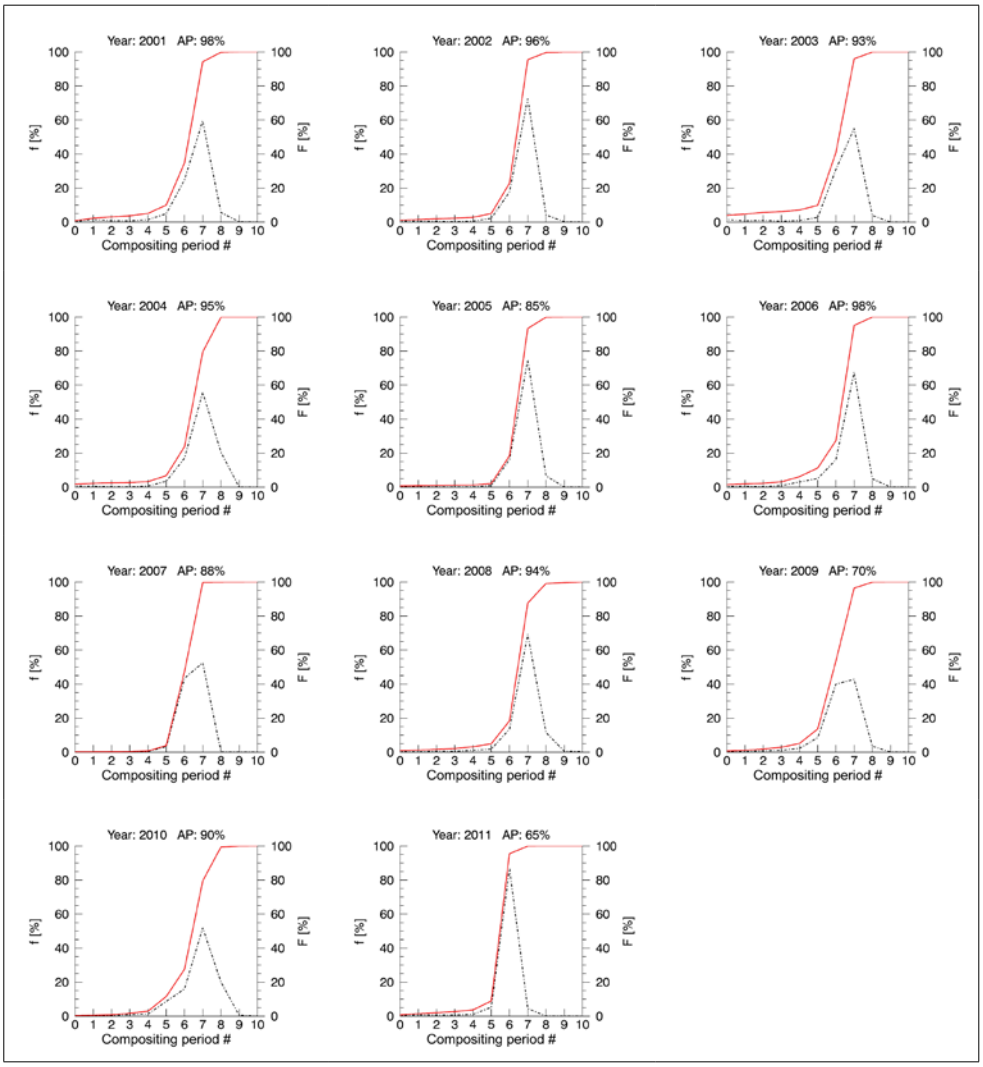

Figure 12 - Relative frequency histograms of SOS images calculated with NVDI-9$_{SMOOTH}$ TS. AP: percentage of available pixels from the study area (pixel whose SOS was found in both NVDI-9$_{SMOOTH}$ and NDVI$_{SMOOTH}$ TS). Dash-dot black lines: relative frequencies (left axis); red solid lines: cumulative relative frequencies histograms (right axis).

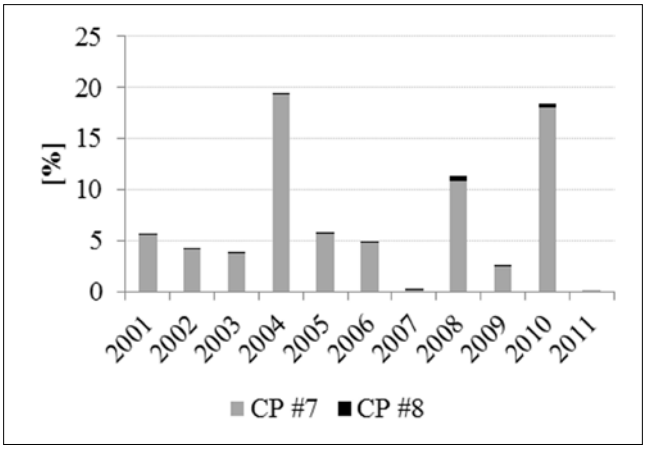

Figure 13 - An extract from relative frequencies histogram: SOS falling on the April RMSE peak (compositing period #7 and #8).

RMSE between corrected and non-corrected TS was found to be greater than the NDVI sensitivity threshold throughout the year, with a peak in April, except in the May-to-September months. This demonstrated that NDVI values were significantly affected by the correction process in the periods during which the start or end of season (EOS) may fall. Some further elements regarding SOS estimation using the threshold-based method implemented in TIMESAT were considered. First, the amount of pixels whose ΔSOS is considered significant ranges from 2% to 31% if the admitted error is ±7 days, and from 48% to 84% if it is restricted to ±2 days. Secondly, the amount of SOS falling around the April RMSE peak is limited (20% maximum, according to the considered year). These results could vary considerably using a different SOS determination method [White et al., 2009], like these based on derivatives of the fitting function [Zhang et al., 2003; Soudani et al., 2008; White et al., 2009; Colombo et al., 2011; Hmimina et al., 2013]. Moreover, validation of SOS estimates should be done with respect to ground data, but these were unavailable for the study area.

Conclusions

This work showed that the correction of MOD13Q1 NDVI TS using actual acquisition dates determined appreciable changes in NDVI values along most of the year, especially when phenological phases (SOS, EOS) were expected to occur. These changes affected a variable, but non-negligible, amount of pixels when the corrected TS was used.

Acknowledgment

Acknowledgments are due to Prof. Luigi Boschetti for his precious advice and suggestions given during the elaboration of this work. Authors are grateful to the referees that spent their valuable time helping to improve this manuscript and to Chris “Otto”, James Snyder and Peter Schlesinger for the manuscript’s language revision. Authors want to thank the staff of the European Journal of Remote Sensing for the kind collaboration during the review and

publication process. The MOD13Q1 data product was obtained through the online Data Pool at the NASA Land Processes Distributed Active Archive Center (LP DAAC), USGS/ Earth Resources Observation and Science (EROS) Center, Sioux Falls, South Dakota (https://lpdaac.usgs.gov/data_access).

Bibliography

Ahl D.E., Gower S.T., Burrows S.N., Shabanov N.V., Myneni R.B., Knyazikhin Y. (2006) - *Monitoring spring canopy phenology of a deciduous broadleaf forest using MODIS*. Remote Sensing of Environment, 104: 88-95. doi: http://dx.doi.org/10.1016/j.rse.2006.05.003.

Boschetti M., Stroppiana D., Brivio P.A., Bocchi S. (2009) - *Multi-year monitoring of rice crop phenology through time series analysis of MODIS images*. International Journal of Remote Sensing, 30: 4643-4662. doi: http://dx.doi.org/10.1080/01431160802632249.

Bradley N.L., Leopold A.C., Ross J., Huffaker W. (1999) - *Phenological changes reflect climate change in Wisconsin.* Proceedings of the National Academy of Sciences of the United States of America, 96: 9701-9704. doi: http://dx.doi.org/10.1073/pnas.96.17.9701.

Brügger R., Dobbertin M., Krauchi N. (2003) - *Phenological variation of forest trees*. Phenology: an Integrative Environmental Science, 39: 255-267. doi: http://dx.doi.org/10.1007/978-94-007-0632-3_16.

Busetto L., Colombo R., Migliavacca M., Cremonese E., Meroni M., Galvagno M., Rossini M., Siniscalco C., Di Cella U.M., Pari E. (2010) - *Remote sensing of larch phenological cycle and analysis of relationships with climate in the Alpine region*. Global Change Biology, 16: 2504-2517. doi: http://dx.doi.org/10.1111/j.1365-2486.2010.02189.x.

Colombo R., Busetto L., Fava F., Di Mauro B., Migliavacca M., Cremonese E., Galvagno M., Rossini M., Meroni M., Cogliati S., Panigada C., Siniscalco C., di Cella U.M. (2011) - *Phenological monitoring of grassland and larch in the Alps from Terra and Aqua MODIS images*. Italian Journal of Remote Sensing, 43: 83-96. doi: http://dx.doi.org/10.5721/ItJRS20114336.

Colombo R., Busetto L., Migliavacca M., Cremonese E., Meroni M., Galvagno M., Rossini M., Siniscalco C., di Cella U.M. (2009) - *On the spatial and temporal variability of Larch phenological cycle in mountainous areas*. Rivista Italiana Di Telerilevamento, 41: 79-96.

Cowie J. (2007) - *Climate Change: Biological and Human Aspects*. Cambridge University Press, pp. 487. doi: http://dx.doi.org/10.1017/CBO9780511803826.

Crucifix M., Betts R.A., Cox P.M. (2005) - *Vegetation and climate variability: a GCM modelling study*. Climate Dynamics, 24: 457-467. doi: http://dx.doi.org/10.1007/s00382-004-0504-z.

Elvidge C.D., Chen Z.K. (1995) - *Comparison of broad-band and narrow-band red and near-infrared vegetation indexes*. Remote Sensing of Environment, 54: 38-48. doi: http://dx.doi.org/10.1016/0034-4257(95)00132-K.

Fabian P., Menzel A. (1998) - *Changes in phenology of trees in Europe*. International Seminar on Causes and Consequences of Accelerating Tree Growth in Europe. Nancy, France, pp. 43-51.

Gottero F., Ebone A., Terzuolo P.G., Camerano P. (2007) - *I boschi del Piemonte. San Mauro*

(TO): Regione Piemonte - Assessorato allo sviluppo della montagna e foreste, opere pubbliche, difesa del suolo - Direzione Economia Montana e Foreste - Settore Politiche Forestali.

Gu L.H., Post W.M., Baldocchi D., Black T.A., Verma S.B., Vesala T., Wofsy S.C. (2003) - *Phenology of vegetation photosynthesis*. Phenology: an Integrative Environmental Science, 39: 467-485.

Gutman G., Ignatov A., Olson S. (1995) - *Global land monitoring using AVHRR time-series*. Advances in Space Research, 17: 51-54. doi: http://dx.doi.org/10.1016/0273-1177(95)00445-K.

Hird J.N., McDermid G.J. (2009) - *Noise reduction of NDVI time series: An empirical comparison of selected techniques*. Remote Sensing of Environment, 113: 248-258. doi: http://dx.doi.org/10.1016/j.rse.2008.09.003.

Hmimina G., Dufrene E., Pontailler J.Y., Delpierre N., Aubinet M., Caquet B., de Grandcourt A., Burban B., Flechar C., Granier A., Gross P., Heinesch B., Longdoz B., Moureaux C., Ourcival J.M., Rambal S., Saint Andre L., Soudani K. (2013) - *Evaluation of the potential of MODIS satellite data to predict vegetation phenology in different biomes: An investigation using ground-based NDVI measurements*. Remote Sensing of Environment, 132: 145-158. doi: http://dx.doi.org/10.1016/j.rse.2013.01.010.

Huete A., Didan K., Miura T., Rodriguez E.P., Gao X., Ferreira L.G. (2002) - *Overview of the radiometric and biophysical performance of the MODIS vegetation indices*. Remote Sensing of Environment, 83: 195-213. doi: http://dx.doi.org/10.1016/S0034-4257(02)00096-2.

Huete A., Justice C., van Leeuwen W. (1999) - *MODIS vegetation index (MOD13) Algorithm Theoretical Basis Document Version 3*. University of Arizona and University of Virginia.

Jackson R.D., Huete A.R. (1991) - *Interpreting vegetation indexes*. Preventive Veterinary Medicine, 11: 185-200. doi: http://dx.doi.org/10.1016/S0167-5877(05)80004-2.

Jarvis A.R., H.I.Nelson, A.Guevara, E. (2008) - *Hole-filled seamless SRTM data V4*. International Centre for Tropical Agriculture (CIAT).

Jönsson P., Eklundh L. (2002) - *Seasonality extraction by function fitting to time-series of satellite sensor data*. IEEE Transactions on Geoscience and Remote Sensing, 40: 1824-1832. doi: http://dx.doi.org/10.1109/TGRS.2002.802519.

Jönsson P., Eklundh L. (2003) - *Seasonality extraction from satellite sensor data*. Chen C.H. (Ed.), Frontiers of Remote Sensing Information Processing, World Scientific Publishing, pp. 487-500.

Jönsson P., Eklundh L. (2004) - *TIMESAT - a program for analyzing time-series of satellite sensor data*. Computers & Geosciences, 30: 833-845. doi: http://dx.doi.org/10.1016/j.cageo.2004.05.006.

Karlsen S.R., Ramfjord H., Hogda K.A., Johansen B., Danks F.S., Brobakk T.E. (2009) - *A satellite-based map of onset of birch (Betula) flowering in Norway*. Aerobiologia, 25: 15-25. doi: http://dx.doi.org/10.1007/s10453-008-9105-3.

Karlsen S.R., Tolvanen A., Kubin E., Poikolainen J., Hogda K.A., Johansen B., Danks F.S., Aspholm P., Wielgolaski F.E., Makarova O. (2008) - *MODIS-NDVI-based mapping of the length of the growing season in northern Fennoscandia*. International Journal of Applied Earth Observation and Geoinformation, 10: 253-266. doi: http://dx.doi.org/10.1016/j.jag.2007.10.005.

Liang L., Schwartz M.D., Fei S. (2011) - *Validating satellite phenology through intensive*

ground observation and landscape scaling in a mixed seasonal forest. Remote Sensing of Environment, 115: 143-157. doi: http://dx.doi.org/10.1016/j.rse.2010.08.013.

Lieth H. (1974) - *Ecological studies analysis and synthesis vol 8 phenology and seasonality modeling. Ecological Studies*. Lieth H. (Ed). Analysis and Synthesis, Phenology and Seasonality Modeling, 8: XV+444. Illus. Maps. Springer-Verlag: New York, N.Y., U.S.A. doi: http://dx.doi.org/10.1007/978-3-642-51863-8.

MODIS Land Team (2011) - *Status for: Vegetation Indices (MOD13)* - General Accuracy Statement.

Noormets A. (2009) - *Phenology of Ecosystem Processes: Applications in Global Change Research*. Noormets, Asko (Ed.). Springer, New York, pp. XV+275.

Nordli O., Wielgolaski F.E., Bakken A.K., Hjeltnes S.H., Mage F., Sivle A., Skre O. (2008) - *Regional trends for bud burst and flowering of woody plants in Norway as related to climate change*. International Journal of Biometeorology, 52: 625-639. doi: http://dx.doi.org/10.1007/s00484-008-0156-5.

Pena-Barragan J.M., Ngugi M.K., Plant R.E., Six J. (2011) - *Object-based crop identification using multiple vegetation indices, textural features and crop phenology*. Remote Sensing of Environment, 115: 1301-1316. doi: http://dx.doi.org/10.1016/j.rse.2011.01.009.

Peñuelas J., Filella I. (2001) - *Phenology - Responses to a warming world*. Science, 294: 793-794. doi: http://dx.doi.org/10.1126/science.1066860.

Peñuelas J., Rutishauser T., Filella I. (2009) - *Phenology Feedbacks on Climate Change*. Science, 324: 887-888. doi: http://dx.doi.org/10.1126/science.1173004.

Reed B.C., White M., Brown J.F. (2003) - *Remote sensing phenology*. Phenology: an Integrative Environmental Science, Schwartz M.D. (Ed.) Kluwer Academic Publishers, New York, NY pp. 365-381. doi: http://dx.doi.org/10.1007/978-94-007-0632-3_23.

Richardson A.D., Keenan T.F., Migliavacca M., Ryu Y., Sonnentag O., Toomey M. (2013) - *Climate change, phenology, and phenological control of vegetation feedbacks to the climate system*. Agricultural and Forest Meteorology, 169: 156-173. doi: http://dx.doi.org/10.1016/j.agrformet.2012.09.012.

Rousseeuw P.J., Croux C. (1993) - *Alternatives to the median absolute deviation*. Journal of the American Statistical Association, 88: 1273-1283. doi: http://dx.doi.org/10.1080/01621459.1993.10476408.

Schwartz M.D. (1998) - *Green-wave phenology*. Nature: 394: 839-840. doi: http://dx.doi.org/10.1038/29670.

Schucknecht A., Erasmi S., Niemeyer I., Matschullat J. (2013) - *Assessing vegetation variability and trends in north-eastern Brazil using AVHRR and MODIS NDVI time series.* European Journal of Remote Sensing, 46: 40-59. doi: http://dx.doi.org/ 10.5721/EuJRS20134603.

Sesnie S.E., Dickson B.G., Rosenstock S.S., Rundall J.M. (2012) - *A comparison of Landsat TM and MODIS vegetation indices for estimating forage phenology in desert bighorn sheep (Ovis canadensis nelsoni) habitat in the Sonoran Desert, USA*. International Journal of Remote Sensing, 33: 276-286. doi: http://dx.doi.org/10.1080/01431161.2011.592865.

Solano R., Didan K., Jacobson A., Huete A. (2010) - *MODIS Vegetation Index User's Guide (MOD13 Series)*. In, Version 2.00, May 2010 (Collection 5): Vegetation Index and Phenology Lab - The University of Arizona.

Song Y., Njoroge J.B., Morimoto Y. (2013) - *Drought impact assessment from monitoring the seasonality of vegetation condition using long-term time-series satellite images: a*

case study of Mt. Kenya region. Environmental Monitoring and Assessment, 185: 4117-4124. doi: http://dx.doi.org/10.1007/s10661-012-2854-z.

Soudani K., Francois C., le Maire G., Le Dantec V., Dufrene E. (2006) - *Comparative analysis of IKONOS, SPOT, and ETM+ data leaf area index estimation in temperature coniferous and deciduous forest stands*. Remote Sensing of Environment, 102: 161-175. doi: http://dx.doi.org/10.1016/j.rse.2006.02.004.

Soudani K., le Maire G., Dufrene E., Francois C., Delpierre N., Ulrich E., Cecchini S. (2008) - *Evaluation of the onset of green-up in temperate deciduous broadleaf forests derived from Moderate Resolution Imaging Spectroradiometer (MODIS) data*. Remote Sensing of Environment, 112: 2643-2655. doi: http://dx.doi.org/10.1016/j.rse.2007.12.004.

Stroppiana D., Antoninetti M., Brivio P. A. (2014) - *Seasonality of MODIS LST over Southern Italy and correlation with land cover, topography and solar radiation*. European Journal of Remote Sensing, 47: 133-152. doi: http://dx.doi.org/10.5721/EuJRS20144709.

Wang H., Lin H., Chen J., Chen F. (2012) - *Study on the relationship between sub-pixel percentage cover and multi-temporal NDVI*. International Journal of Remote Sensing, 33: 5615-5628. doi: http://dx.doi.org/10.1080/01431161.2012.666813.

White M.A., de Beurs K.M., Didan K., Inouye D.W., Richardson A.D., Jensen O.P., O'Keefe J., Zhang G., Nemani R.R., van Leeuwen W.J.D., Brown J.F., de Wit A., Schaepman M., Lin X., Dettinger M., Bailey A.S., Kimball J., Schwartz M.D., Baldocchi D.D., Lee J.T., Lauenroth W.K. (2009) - *Intercomparison, interpretation, and assessment of spring phenology in North America estimated from remote sensing for 1982-2006*. Global Change Biology, 15: 2335-2359. doi: http://dx.doi.org/10.1111/j.1365-2486.2009.01910.x.

Xu K., Zhang X., Chen B., Hua K., Zheng K., Wu T. (2011) - *MODIS NDVI data to monitor the growing season of the deciduous forest in Beijing, China*. Conference on Earth Resources and Environmental Remote Sensing/GIS Applications II. Prague, Czech Republic.

Zhang X.Y., Friedl M.A., Schaaf C.B., Strahler A.H., Hodges J.C.F., Gao F., Reed B.C., Huete, A. (2003) - *Monitoring vegetation phenology using MODIS*. Remote Sensing of Environment, 84 (3): 471-475. doi: http://dx.doi.org/10.1016/S0034-4257(02)00135-9.